Journal of Mechanical Science and Technology 28 (9) (2014) 3741~3747
www.springerlink.com/content/1738-494x
DOI 10.1007/s12206-014-0835-6

Vibration of nonuniform carbon nanotube with attached mass via nonlocal Timoshenko beam theory †

Hai-Li Tang, Zhi-Bin Shen* and Dao-Kui Li*

College of Aerospace Science and Engineering, National University of Defense Technology, Changsha, Hunan 410073, China

(Manuscript Received August 28, 2013; Revised May 4, 2014; Accepted May 27, 2014)

Abstract

This paper studies the vibrational behavior of nonuniform single-walled carbon nanotube (SWCNT) carrying a nanoparticle. A nonuniform cantilever beam with a concentrated mass at the free end is analyzed according to the nonlocal Timoshenko beam theory. A governing equation of a nonuniform SWCNT with attached mass is established. The transfer function method incorporating with the perturbation method is utilized to obtain the resonant frequencies of a vibrating nonlocal cantilever-mass system. The effects of the nonlocal parameter, taper ratio and attached mass on the natural frequencies and frequency shifts are discussed. Obtained results indicate that the sensitivity of the frequency shifts on the attached mass increases when the length-to-diameter ratio decreases. Tapered SWCNT possesses higher fundamental frequencies if the taper ratio becomes larger.

Keywords: Nonuniform SWCNT; Mass sensor; Nonlocal Timoshenko beam theory; Transfer function method; Perturbation method

1. Introduction

Carbon nanotubes (CNTs) have attracted increasing attention of researchers since their discovery [1] in 1991, and owing to their unique properties [2] they have potential and evolving applications [3]. Nanoscale mass sensors are based on the fact that the change in the natural frequencies is sensitive to attached masses. Therefore, a key issue of mass detection is to quantify the change in resonant frequencies or frequency shift due to attached masses. Nanoparticle detection including gas detection, virus detection and charge detection requires extra-high mass sensitivity. The vibration frequencies of CNTs reaching THz and their high sensitivity to environment change make it possible to fabricate nanoscale mass sensors [4, 5].

As we know, the geometry of mechanical devices strongly affects their dynamics behaviors. Consequently, for various purposes, a variety of CNTs such as single-, double-, and multi-walled, as well as Y-, bamboo-, cone-shaped, horn-shaped CNTs [6-10] have been synthesized. Nonuniform CNTs possess varying cross-section and are one of the most attractive shapes of CNTs. On the other hand, mass sensors with varying cross-section have some advantages over those with uniform cross-section. Therefore, it is extremely necessary to study the vibration performance of mass sensors made of nonuniform CNTs.

Generally, the theoretical analysis of CNTs is classified into two main categories, the discrete atomic modeling and the continuum modeling. In addition, experimental evidence [11] has showed pronounced size effects in CNTs. Atomic modeling such as molecular dynamics simulation are more suitable in accurately describing size-dependent mechanical properties. However, these discrete simulations are limited to systems with a small number of molecules and atoms and therefore restricted to small-scale modeling. Moreover, it is extraordinary hard to conduct experimental tests efficiently at nanoscale. To overcome these deficiencies, modified continuum mechanics approaches, the nonlocal elasticity theory [12] describing long-range interactions of the nanoscale effect, has been widely accepted to deal with size-dependent problems. In this way, a lot of researches have been reported on the vibration of CNTs with an attached mass based on the nonlocal Euler-Bernoulli beam theory (EBT) [13] and Timoshenko beam theory (TBT) [14, 15]. It is mentioned that all of these studies are only suitable for uniform CNTs with attached mass. For nonuniform CNTs, free vibration analyses without considering shear deformation and rotary inertia of the cross-section have been made by Lee and Chang [16], Murmu and Pradhan [17], respectively. For nonuniform nanocantilever with attached nanoparticle, Tang et al. [18] investigated the vibration of horn-shaped single wall CNT (SWCNTs) based on the nonlocal EBT. However, there are few studies on resonant frequency of vibration of a nonuniform CNT-based mass

*Corresponding author. Tel.: +86 731 84573178, Fax.: +86 731 84512301
E-mail address: zb_shen@yeah.net (Z.B.Shen); lidaokui@nudt.edu.cn (D.K.Li)
† Recommended by Associate Editor Jin Weon Kim

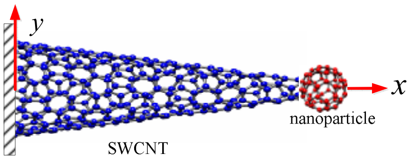

Fig. 1. Nonuniform SWCNT-based mass sensor.

sensor using nonlocal TBT, to the best knowledge of the authors.

The present paper aims at analyzing the vibration response of nonuniform SWCNTs with an attached mass. The nonlocal TBT with the scale parameter is applied. Using the transfer function method (TFM) [19] incorporating with the perturbation method (PM), the natural frequencies of the SWCNT-based mass sensor are evaluated. A detailed investigation is carried out for the effects of the nonlocal parameter, attached mass and geometry parameters on the natural frequencies and frequency shifts.

2. Governing equations and boundary conditions

2.1 Dynamic equation of nonuniform SWCNT-based mass sensors

In this study, a nonuniform SWCNT-based mass sensor can be modeled as a nonuniform cantilever beam of length L and carrying a concentrated mass m at the free tip, as shown in Fig. 1. Its cross section is a circle with radius r varying linearly r_0 to r_L, and the thickness of the pipe retains constant value δ.

Based on the nonlocal TBT, the governing equations of transverse vibration for SWCNTs with varying cross-section can be expressed as

$$\rho A_x \frac{\partial^2 w}{\partial t^2} - \frac{\partial Q}{\partial x} = 0, \quad 0 < x < L \tag{1}$$

$$\rho I_x \frac{\partial^2 \theta}{\partial t^2} - \frac{\partial M}{\partial x} + Q = 0, \quad 0 < x < L \tag{2}$$

where w and θ are the transverse displacement and the rotation of cross-section, both of which depend on the longitudinal coordinate x and time t, ρ the mass density, A_x the area of cross-section, I_x the moment of inertia of cross-sectional area, M the bending moment, and Q the shearing force. For nonuniform SWCNTs, the radius of cross section varies and is assumed to obey

$$r_x = -(r_0 - r_L)x/L + r_0 = \varepsilon x + r_0 \tag{3}$$

then we have

$$A_x = \gamma x + n, \quad (\gamma = 2\varepsilon\delta\pi, \quad n = 2\pi r_0 \delta) \tag{4}$$

$$I_x = 0.25\pi\left[(r_x + 0.5\delta)^4 - (r_x - 0.5\delta)^4\right]. \tag{5}$$

Furthermore, the bending moment M and the shearing force Q based on the nonlocal TBT can be obtained below, respectively

$$M = \rho(e_0 a)^2 \frac{\partial(I_x \theta)}{\partial x}\frac{\partial^2 \theta}{\partial t^2} + \rho(e_0 a)^2 A_x \frac{\partial^2 w}{\partial t^2} + EI_x \frac{\partial \theta}{\partial x} \tag{6}$$

$$Q = \rho(e_0 a)^2 \frac{\partial(A_x w)}{\partial x}\frac{\partial^2 w}{\partial t^2} + \kappa G A_x\left(\theta + \frac{\partial w}{\partial x}\right) \tag{7}$$

where E is Young's modulus, G the shear modulus, $e_0 a$ the nonlocal parameter with length unit which can be used to modify the classical TBT, κ the shear correction coefficient depending on the shape of the cross section. By substituting Eqs. (6) and (7) into Eqs. (1) and (2), then coupled governing equations of the nonlocal TBT can be obtained as follows

$$\begin{aligned}\rho A_x\left(1-(e_0 a)^2\frac{\partial^2}{\partial x^2}\right)\frac{\partial^2 w}{\partial t^2} - \kappa G A_x\left(\frac{\partial \theta}{\partial x} + \frac{\partial^2 w}{\partial x^2}\right) \\ -2\rho(e_0 a)^2 \frac{\partial A_x}{\partial x}\frac{\partial^3 w}{\partial x \partial t^2} - \kappa G \frac{\partial A_x}{\partial x}\left(\theta + \frac{\partial w}{\partial x}\right) = 0\end{aligned} \tag{8}$$

$$\begin{aligned}\rho I_x\left(1-(e_0 a)^2\frac{\partial^2}{\partial x^2}\right)\frac{\partial^2 \theta}{\partial t^2} - EI_x\frac{\partial^2 \theta}{\partial x^2} + \kappa G A_x\left(\theta + \frac{\partial w}{\partial x}\right) \\ -\rho(e_0 a)^2\left(\frac{\partial^2 I_x}{\partial x^2}\frac{\partial^2 \theta}{\partial t^2} + 2\frac{\partial I_x}{\partial x}\frac{\partial^3 \theta}{\partial x \partial t^2}\right) - E\frac{\partial I_x}{\partial x}\frac{\partial \theta}{\partial x} = 0.\end{aligned} \tag{9}$$

2.2 Boundary conditions

For a cantilever beam, the corresponding boundary conditions read

$$w(0,t) = \theta(0,t) = 0, \quad M(L,t) = 0 \tag{10}$$

$$Q(L,t) + m\frac{\partial^2 w(L,t)}{\partial t^2} = 0. \tag{11}$$

Furthermore, the initial state of the sensor is assumed to be at rest, namely

$$w(x,0) = \frac{\partial w(x,0)}{\partial t} = 0, \quad \theta(x,0) = \frac{\partial \theta(x,0)}{\partial t} = 0. \tag{12}$$

Neglecting shear deformation and rotary inertia of the cross-section, the governing equation of transverse vibration based on the nonlocal EBT for SWCNTs with varying cross-section is recovered [18].

3. Solution method

For the uniform Timoshenko beams with attached mass, it is easy to solve the govern equation using TFM [19]. For the present paper, since the governing Eqs. (8) and (9) are related to differential equations with variable coefficients, it is difficult to derive its exact solution directly. PM can be employed to obtain the approximate solution of the nonuniform structures, effectively. In this section, instead we invoke the TFM and the PM to determine the natural frequencies.

3.1 TFM for nonlocal Timoshenko beams

With the aid of the initial conditions Eq. (12), after performing Laplace transform, the governing Eqs. (8) and (9) along with the corresponding boundary conditions (10) and (11) become

$$\rho s^2 A_x\left(1-(e_0a)^2\frac{\partial^2}{\partial x^2}\right)\tilde{w}-\kappa GA_x\left(\frac{\partial\tilde{\theta}}{\partial x}+\frac{\partial^2\tilde{w}}{\partial x^2}\right) - 2\rho(e_0a)^2\gamma s^2\frac{\partial\tilde{w}}{\partial x}-\kappa G\gamma\left(\tilde{\theta}+\frac{\partial\tilde{w}}{\partial x}\right)=0 \tag{13}$$

$$\rho s^2 I_x\left(1-(e_0a)^2\frac{\partial^2}{\partial x^2}\right)\tilde{\theta}-EI_x\frac{\partial^2\tilde{\theta}}{\partial x^2}+\kappa GA_x\left(\tilde{\theta}+\frac{\partial\tilde{w}}{\partial x}\right) - \rho(e_0a)^2s^2\left(\tilde{\theta}\frac{\partial}{\partial x}+2\frac{\partial\tilde{\theta}}{\partial x}\right)\frac{\partial I_x}{\partial x}-E\frac{\partial I_x}{\partial x}\frac{\partial\tilde{\theta}}{\partial x}=0 \tag{14}$$

and

$$\tilde{w}(0,s)=\tilde{\theta}(0,s)=0 \tag{15}$$

$$\rho(e_0a)^2s^2\left(\gamma\tilde{w}+A_L\frac{\partial\tilde{w}}{\partial x}\right)+\kappa GA_L\left(\tilde{\theta}+\frac{\partial\tilde{w}}{\partial x}\right)+ms^2\tilde{w}=0 \tag{16}$$

$$\rho(e_0a)^2s^2\left(\tilde{\theta}\frac{\partial I_x}{\partial x}\Big|_{x=L}+I_L\frac{\partial\tilde{\theta}}{\partial x}+A_L\tilde{w}\right)+EI_L\frac{\partial\tilde{\theta}}{\partial x}=0 \tag{17}$$

where s is the Laplace transform parameter.

To facilitate our treatment, we introduce the following dimensionless parameters

$$\tilde{W}=\tilde{w}/L,\ \ X=x/L,\ \ \lambda=e_0a/L,\ \ \mu=m/\rho A_L L,$$
$$\Gamma_s=\rho A_x L^4 s^2/\left(EI_x\right),\ \ \Gamma_{\mathrm{P}}=\rho\gamma L^5 s^2/\left(EI_x\right),$$
$$\Gamma_{\mathrm{P}L}=\rho\gamma L^5 s^2/\left(EI_L\right),\ \ \Gamma_{sL}=\rho A_L L^4 s^2/\left(EI_L\right),$$
$$\Psi_s=\rho L^2 s^2/E,\ \ \Gamma_x=\rho A_x L^4 s_0/\left(EI_x\right),$$
$$\beta_x=kGA_xL^2/\left(EI_x\right),\ \ \beta_{\mathrm{P}}=kG\gamma L^3/\left(EI_x\right),$$
$$\alpha_x=I_x/\left(A_xL^2\right),\ \ \chi_L=2\pi\delta L/A_0,$$
$$\phi_x=4r_0x/\left[\left(r_0+0.5\delta\right)^2+\left(r_0-0.5\delta\right)^2\right],$$
$$T_x=L\left[\left(r_x+0.5\delta\right)^3-\left(r_x-0.5\delta\right)^3\right]/\left[\left(r_x+0.5\delta\right)^4-\left(r_x-0.5\delta\right)^4\right]$$

where s_0 is a reference value related to the Laplace transform parameter s.

Next, after substituting the dimensionless parameters above into Eqs. (13)-(17) and introducing a state vector as

$$\boldsymbol{\eta}(X,s)=\left[\tilde{W}(X,s),\frac{\partial\tilde{W}(X,s)}{\partial X},\tilde{\theta}(X,s),\frac{\partial\tilde{\theta}(X,s)}{\partial X}\right]^{\mathrm{T}} \tag{18}$$

where the superscript T denotes matrix transpose, Eqs. (13) and (14) together with Eqs. (15)-(17) can be rewritten in a matrix form below, respectively

$$\frac{\partial\boldsymbol{\eta}(X,s)}{\partial X}=\mathbf{F}(X,s)\boldsymbol{\eta}(X,s) \tag{19}$$

$$\mathbf{M}(s)\boldsymbol{\eta}(0,s)+\mathbf{N}(s)\boldsymbol{\eta}(1,s)=0 \tag{20}$$

where $\mathbf{F}(X,s)$, $\mathbf{M}(s)$ and $\mathbf{N}(s)$ are all 4×4 matrixes and given in Appendix **A**.

Thus the problem under consideration is then reduced to solving ordinary differential Eq. (19) of first order subject to the condition Eq. (20).

3.2 Perturbation solution for nonlocal Timoshenko beam

To obtain approximate solutions of differential Eq. (19) with varying coefficients, we invoke the PM. To this end, a dimensionless parameter ε is defined as $\varepsilon=\left(r_L-r_0\right)/L$, and we have

$$s^2=s_0+\varepsilon s_1 \tag{21}$$

$$\boldsymbol{\eta}(X,s)=\boldsymbol{\eta}_0(X,s_0)+\varepsilon\boldsymbol{\eta}_1(X,s_0,s_1) \tag{22}$$

$$\mathbf{F}(X,s)=\mathbf{F}_0(s_0)+\varepsilon\mathbf{F}_1(X,s_0,s_1) \tag{23}$$

$$\mathbf{N}(s)=\mathbf{N}_0(s_0)+\varepsilon\mathbf{N}_1(s_0,s_1) \tag{24}$$

where s_1 is a parameter related to the Laplace transform parameter s. For simplicity, only first order perturbation solution is used in the present study.

Substituting Eqs. (21)-(24) into Eqs. (19) and (20) and equating the coefficient of each power of ε to zero, we have

$$\begin{cases}\dfrac{\partial\boldsymbol{\eta}_0(X,s_0)}{\partial X}=\mathbf{F}_0(s_0)\boldsymbol{\eta}_0(X,s_0)\\ \mathbf{M}\boldsymbol{\eta}_0(0,s_0)+\mathbf{N}_0(s_0)\boldsymbol{\eta}_0(1,s_0)=0\end{cases} \tag{25}$$

$$\begin{cases}\dfrac{\partial\boldsymbol{\eta}_1(X,s_0,s_1)}{\partial X}=\mathbf{F}_0(s_0)\boldsymbol{\eta}_1(X,s_0,s_1)+\mathbf{F}_1(X,s_0,s_1)\boldsymbol{\eta}_0(X,s_0)\\ \mathbf{M}\boldsymbol{\eta}_1(0,s_0,s_1)+\mathbf{N}_0(s_0)\boldsymbol{\eta}_1(1,s_0,s_1)+\mathbf{N}_1(s_0,s_1)\boldsymbol{\eta}_0(1,s_0)=0\end{cases} \tag{26}$$

where $\mathbf{F}_0(s_0)$, $\mathbf{N}_0(s_0)$, $\mathbf{F}_1(X,s_0,s_1)$ and $\mathbf{N}_1(s_0,s_1)$ are all 4×4 matrixes and given in Appendix **B**, and we also denote

$$\mathbf{F}_1(X,s_0,s_1)=\mathbf{F}_{10}+\mathbf{F}_{11}s_1,\ \ \mathbf{N}_1(s_0,s_1)=\mathbf{N}_{10}+\mathbf{N}_{11}s_1.$$

Finally, the natural frequencies can be obtained by

$$f=\frac{\omega}{2\pi}=\frac{\sqrt{-s_0-\varepsilon s_1}}{2\pi}. \tag{27}$$

Considering the fact that Eqs. (25) and (26) are ordinary differential equations with constant coefficients, rather than varying coefficients, we can easily determine the solutions of Eqs. (25) and (26), respectively. That is, the solution to Eq. (25) is readily obtained to be

$$\det\left[\mathbf{M}+\mathbf{N}_0(s_0)\mathrm{e}^{\mathbf{F}_0(s_0)}\right]=0\,. \tag{28}$$

Hence, the zeroth-order perturbation of the circular frequency $\omega_0=\sqrt{-s_0}$, and the corresponding modal shape can be evaluated by

$$\boldsymbol{\eta}_0(X,s_0)=\mathrm{e}^{\mathbf{F}_0(s_0)X}\mathbf{V}_0 \tag{29}$$

where V_0 is the eigenvector corresponding to the matrix $\mathbf{M}+\mathbf{N}_0(s_0)\mathrm{e}^{\mathbf{F}_0(s_0)}$ with zero as its eigenvalue.

To obtain its first-order perturbation solution, we express the solution to Eq. (26) according to TFM

$$\boldsymbol{\eta}_1(X,s_0,s_1)=\mathrm{e}^{\mathbf{F}_0(s_0)X}\left[\int_0^X \mathrm{e}^{-\mathbf{F}_0(s_0)\xi}\mathbf{F}_1(\xi,s_0,s_1)\boldsymbol{\eta}_0(\xi,s_0)d\xi+\mathbf{A}_0\right]. \tag{30}$$

Inserting $\mathbf{F}_1(X,s_0,s_1)=\mathbf{F}_{10}+\mathbf{F}_{11}s_1$ together with Eq. (29) into Eq. (30) leads to

$$\boldsymbol{\eta}_1(X,s_0,s_1)=\mathrm{e}^{\mathbf{F}_0(s_0)X}\mathbf{V}_{10}+s_1\mathrm{e}^{\mathbf{F}_0(s_0)X}\mathbf{V}_{11}+\mathrm{e}^{\mathbf{F}_0(s_0)X}\mathbf{A}_0 \tag{31}$$

where

$$\mathbf{V}_{10}=\int_0^X \mathrm{e}^{-\mathbf{F}_0(s_0)\xi}\mathbf{F}_{10}\mathrm{e}^{\mathbf{F}_0(s_0)\xi}\mathbf{V}_0 d\xi\ ,\quad \mathbf{V}_{11}=\int_0^X \mathrm{e}^{-\mathbf{F}_0(s_0)\xi}\mathbf{F}_{11}\mathrm{e}^{\mathbf{F}_0(s_0)\xi}\mathbf{V}_0 d\xi\,. \tag{32}$$

Consequently, substituting $\mathbf{N}_1(s_0,s_1)=\mathbf{N}_{10}+\mathbf{N}_{11}s_1$ and Eq. (31) into the second equation in Eq. (26) yields

$$\begin{aligned}&\left(\mathbf{M}+\mathbf{N}_0(s_0)\mathrm{e}^{\mathbf{F}_0(s_0)}\right)\mathbf{A}_0+s_1\left(\mathbf{N}_0(s_0)\mathrm{e}^{\mathbf{F}_0(s_0)}\mathbf{V}_{11}+\mathbf{N}_{11}\mathrm{e}^{\mathbf{F}_0(s_0)}\mathbf{V}_0\right)\\&\qquad+\mathbf{N}_0(s_0)\mathrm{e}^{\mathbf{F}_0(s_0)}\mathbf{V}_{10}+\mathbf{N}_{10}\mathrm{e}^{\mathbf{F}_0(s_0)}\mathbf{V}_0=0\,.\end{aligned} \tag{33}$$

By rewriting $\mathbf{M}+\mathbf{N}_0(s_0)\mathrm{e}^{\mathbf{F}_0(s_0)}=\left[\mathbf{P}\right]\left[\lambda_0\right]\left[\mathbf{P}\right]^{-1}$ and left multiplying Eq. (33) by $\left[\mathbf{P}\right]^{-1}$, one gets

$$\begin{aligned}&\left[\lambda_0\right]\left[\mathbf{P}\right]^{-1}\mathbf{A}_0+s_1\left[\mathbf{P}\right]^{-1}\left(\mathbf{N}_0(s_0)\mathrm{e}^{\mathbf{F}_0(s_0)}\mathbf{V}_{11}+\mathbf{N}_{11}\mathrm{e}^{\mathbf{F}_0(s_0)}\mathbf{V}_0\right)\\&\qquad+\left[\mathbf{P}\right]^{-1}\left[\mathbf{N}_0(s_0)\mathrm{e}^{\mathbf{F}_0(s_0)}\mathbf{V}_{10}+\mathbf{N}_{10}\mathrm{e}^{\mathbf{F}_0(s_0)}\mathbf{V}_0\right]=0\end{aligned} \tag{34}$$

where $\left[\lambda_0\right]$ and $\left[\mathbf{P}\right]$ are diagonal matrixes consisting of eigenvalues and eigenvectors, respectively. Obviously, there must exist a zero-eigenvalue in $\left[\lambda_0\right]$. s_1 in Eq. (27) can be then obtained easily by solving Eq. (34), and the first-order perturbation solution is then determined.

Table 1. Comparison of the natural frequencies (GHz) obtained from TFM & PM with those using FEM software for a SWCNT-based mass sensor with L = 22 nm and r_0 = 0.8 nm.

c	m/g		1	3	5
1/4	0	TFM&PM	14.4238	199.0966	546.4015
		FEM	14.5396	201.1667	558.1628
		%Error	0.7964	1.0290	2.1071
	10^{-21}	TFM&PM	13.9968	193.8567	534.5559
		FEM	14.1113	195.7882	545.7362
		%Error	0.8114	0.9865	2.0487
1/8	0	TFM&PM	14.2111	208.1089	566.7282
		FEM	14.2528	211.1869	582.3247
		%Error	0.2926	1.4575	2.6783
	10^{-21}	TFM&PM	13.8460	203.6253	556.4650
		FEM	13.8864	206.4349	571.3588
		%Error	0.2909	1.3610	2.6067
0	0	TFM&PM	13.9952	216.7468	586.3507
		FEM	14.0169	220.6942	604.3092
		%Error	0.1548	1.7886	2.9717
	10^{-21}	TFM&PM	13.6776	212.7577	577.7908
		FEM	13.6974	216.4300	594.5050
		%Error	0.1446	1.6968	2.8114

4. Numerical results and discussion

In this section, to show the influences of some parameters on the resonance frequencies or frequencies shift, an example of a nonuniform SWCNT with an attached mass is presented and numerical results of the resonance frequencies and frequency shifts are calculated. In the following computations, the material properties and geometry of a SWCNT are chosen as follows: Young's modulus $E=1\text{TPa}$, Poisson's ratio $\nu=0.3$, the shear correction coefficient $\kappa=2(1+\nu)/(4+3\nu)$, the mass density $\rho=2.24\text{g}/\text{cm}^3$, the effective tube thickness $\delta=0.34$ nm , the radius at the clamped end 0.8nm unless otherwise stated. For convenience, we denote the taper ratio as c = 1-r_L/r_0, which varies from 0 to 0.5 for the present study.

4.1 Result validation

Prior to the presentation of numerical results, let us examine the accuracy and validity of the present approach. This is done by comparing our numerical results with those obtained from FEM software MSC.Nastran for the case of e_0a = 0, which are tabulated in Table 1. It can be seen that our results and the FEM simulation results are in good agreement. The maximum relative error for the fundamental frequencies is 0.8114%. This means that the present approach is suitable for analyzing cantilevered nonuniform SWCNTs with a concentrated mass at the free end.

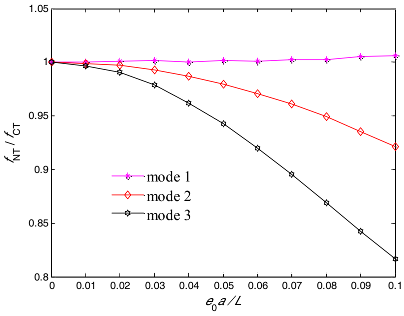

Fig. 2. Nonlocal effect on the natural frequency for different vibration modes of a nonuniform SWCNT with μ = 0, L = 22 nm and c = 0.25.

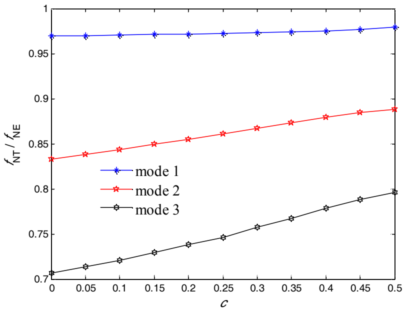

Fig. 3. Effects of transverse shear deformation and rotary inertia on natural frequencies for a nonuniform SWCNT with e_0a/L = 0.05, μ = 0, L = 12 nm and r_0 = 0.8 nm.

4.2 Study of natural frequencies

In the absence of attached mass, Fig. 2 shows the effect of the nonlocal parameter on the natural frequencies for different vibration modes, where the frequencies with the subscripts NT and CT stand for those corresponding to the nonlocal and classical TBT, respectively. From Fig. 2, the nonlocal effect is found to be more apparent with an increase of e_0a / L. Moreover, this effect depends on the vibration modes. The higher the vibration order is, the more apparent the nonlocal effect is.

In addition, the effects of transverse shear deformation and rotary inertia on vibration frequencies for nonuniform SWCNTs are investigated in Fig. 3. For comparison of the natural frequencies between nonlocal Timoshenko beams (NT) with nonlocal Euler-Bernoulli beams (NE), Fig. 3 shows the variation of the frequency ratio f_{NT}/f_{NE} against taper ratio c, and the length of a nonuniform SWCNT is taken as L = 12 nm. From Fig. 3, we find that f_{NT}/f_{NE} is always less than unity for all modes. This implies that the frequencies based on the nonlocal EBT are still overestimated, in particular for higher-order modes.

Fig. 4 illustrates the frequency ratio f/f_0 versus the taper ratio c for three different vibration modes using the nonlocal TBT with μ = 0 and e_0a/L = 0.05, where f_0 is the corresponding value when taking $r_0 = r_L$ = 0.8 nm which means c = 0. From Fig. 4, we can see that the frequency ratio is greater

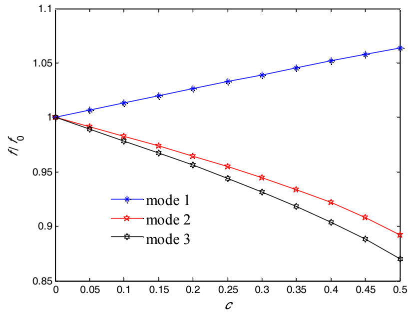

Fig. 4. Taper ratio c effect on the natural frequency ratio f/f_0 of a nonuniform SWCNT with e_0a/L = 0.05, μ = 0, L = 12 nm and r_0 = 0.8 nm.

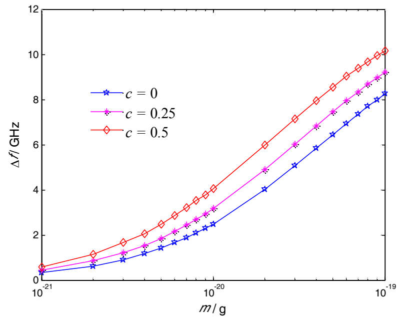

Fig. 5. Taper ratio c effect on the fundamental frequency shift of a nonuniform SWCNT-based mass sensor with e_0a/L = 0.1, L = 22 nm and r_0 = 0.8 nm.

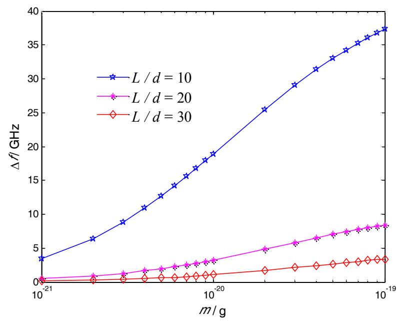

Fig. 6. Length-to-diameter ratio effect on the fundamental frequency shift of a nonuniform SWCNT-based mass sensor with e_0a/L = 0.1, and d = r_0+r_L = 1.2 nm.

than unity and increases with taper ratio increasing for fundamental frequencies, while this trend is opposite for the higher vibration modes. This phenomenon indicates that the nonuniform characteristic can increase fundamental frequencies and reduce higher-order natural frequencies.

4.3 Study of frequency shift

Of much interest is the change in the natural frequencies due to an attached mass. For this purpose, we denote the difference between the natural frequencies with and without attached mass as the frequency shift Δf. Using the nonlocal TBT, Figs. 5 and 6 show the variation of the frequency shift for a nonuniform SWCNT with different taper ratios and length-to-diameter ratios, respectively. It is again viewed that the attached nanoparticle mass increases the frequency shift. From Fig. 5, the frequency shift becomes larger if the taper ratio increases. On the other hand, from Fig. 6 the influence of the length-to-diameter ratio on the frequency shift of shorter nonuniform SWCNTs is more sensitive.

5. Conclusions

In this contribution, the vibration of a nonuniform SWCNT-based mass sensor was studied using the nonlocal TBT. The natural frequencies were determined by the TFM together with the PM. The accuracy and validity of numerical results were verified by a comparison with the corresponding FEM results. The conclusions are given as follows:

The nonlocal effect on the natural frequencies is more apparent with the vibration modes increasing. The taper ratio strongly affects natural frequencies. It increases fundamental frequency and decreases higher order natural frequencies.

Increasing the attached mass or decreasing the length-to-diameter ratio increases the frequency shift. The SWCNT-based mass sensor is more sensitive to the frequency shift if the taper ratio becomes larger.

Acknowledgment

We acknowledge the financial supports of the National Natural Science Foundation of China(No.11302254).

References

[1] S. Iijima, Helical microtubules of graphitic carbon, *Nature,* 354 (1991) 56-58.

[2] E. W. Wong, P. E. Sheehan and C. M. Lieber, Nanobeam mechanics: elasticity, strength, and toughness of nanorods and nanotubes, *Science,* 277 (1997) 1971-1975.

[3] Q. Zheng and Q. Jiang, Multiwalled carbon nanotubes as gigahertz oscillators, *Physical Review Letters,* 88 (2002) 045503.

[4] C. Y. Li and T. W. Chou, Atomistic modeling of carbon nanotube-based mechanical sensors, *Journal of Intelligent Material Systems and Structures,* 17 (2006) 247-254.

[5] R. Chowdhury, S. Adhikari and J. Mitchell, Vibrating carbon nanotube based bio-sensors, *Physica E,* 42 (2009) 104-109.

[6] X. Wu, Y. Tao, C. Mao, L. Wen and J. Zhu, Synthesis of nitrogen-doped horn-shaped carbon nanotubes by reduction of pentachloropyridine with metallic sodium, *Carbon,* 45 (2007) 2253-2259.

[7] S. Y. Sawant, R. S. Somani and H. C. Bajaj, A solvothermal-reduction method for the production of horn shaped multi-wall carbon nanotubes, *Carbon,* 48 (2010) 668-672.

[8] H. C. Su, C. M. Lin, S. J. Yen, Y. C. Chen, C. H. Chen, S. R. Yeh, W. Fang, H. Chen, D. J. Yao, Y. C. Chang and T. R. Yew, A cone-shaped 3D carbon nanotube probe for neural recording, *Biosensors and Bioelectronics,* 26 (2010) 220-227.

[9] P. Soltani, D. D. Ganji, I. Mehdipour and A. Farshidianfar, Nonlinear vibration and rippling instability for embedded carbon nanotubes, *Journal of Mechanical Science and Technology,* 26 (2012) 985-992.

[10] M. H. Kim, S. Seo, W. K. Liu, B. S. Lim, J. B. Choi and M. K. Kim, A modal analysis of carbon nanotube using elastic network model, *Journal of Mechanical Science and Technology,* 26 (2012) 3433-3438.

[11] P. Poncharal, Z. L. Wang, D. Ugarte and W. A. D. Heer, Electrostatic deflections and electro-mechanical resonances of carbon nanotubes, *Science,* 283 (1999) 1513-1516.

[12] A. C. Eringen, *Nonlocal Continuum Field Theories*, Springer, New York (2002).

[13] Z. B. Shen, G. J. Tang, L. Zhang and G. J. Tang, Vibration of double-walled carbon nanotube based nanomechanical sensor with initial axial stress, *Computational Materials Science,* 58 (2012) 51-58.

[14] K. Yun, J. Choi, S. K. Kim and O. Song, Flow-induced vibration and stability analysis of multi-wall carbon nanotubes, *Journal of Mechanical Science and Technology,* 26 (2012) 3911-3920.

[15] Z. B. Shen, D. K. Li, D. Li and G. J. Tang, Frequency shift of a nanomechanical sensor carrying a nanoparticle using nonlocal Timoshenko beam theory, *Journal of Mechanical Science and Technology,* 26 (2012) 1577-1583.

[16] H. L. Lee and W. J. Chang, Surface and small-scale effects on vibration analysis of a nonuniform nanocantilever beam, *Physica E,* 43 (2010) 466-469.

[17] T. Murmu and S. C. Pradhan, Small-scale effect on the vibration of nonuniform nanocantilever based on nonlocal elasticity theory, *Physica E,* 41 (2009) 1451-1456.

[18] H. L. Tang, D. K. Li and S. M. Zhou, Vibration of horn-shaped carbon nanotube with attached mass via nonlocal elasticity theory, *Physica E,* 56 (2014) 306-311.

[19] B. Yang and C. A. Tan, Transfer function of one-dimension distributed parameter system, *ASME Journal of Applied Mechanics,* 59 (1992) 1009-1014.

Appendix

A.1

In Eqs. (19) and (20), the elements of the matrices $F(X,s)$, $M(s)$ and $N(s)$ vanish unless those that are displayed below.

$$\mathbf{F}_{12} = \mathbf{F}_{34} = 1\,,\ \ \mathbf{F}_{21} = \Gamma_s / \left(\lambda^2\Gamma_s + \beta_x\right),$$

$$\mathbf{F}_{22} = -\left(2\lambda^2\Gamma_{\mathrm{p}} + \beta_{\mathrm{p}}\right) / \left(\lambda^2\Gamma_s + \beta_x\right),\ \ \mathbf{F}_{23} = -\beta_{\mathrm{p}} / \left(\lambda^2\Gamma_s + \beta_x\right),$$

$$\mathbf{F}_{24} = -\beta_x / \left(\lambda^2\Gamma_s + \beta_x\right),\ \ \mathbf{F}_{42} = \beta_x / \left(\lambda^2\Psi_s + 1\right),$$

$$\mathbf{F}_{43} = \left(\Gamma_s\alpha_x - \lambda^2 I_x'' L^2\Psi_s / I_x + \beta_x\right) / \left(\lambda^2\Psi_s + 1\right),$$

$$\mathbf{F}_{44} = -I_x' L\left(2\lambda^2\Psi_s + 1\right) / I_x / \left(\lambda^2\Psi_s + 1\right).$$

$$\mathbf{M}_{11} = \mathbf{M}_{23} = 1\,,\ \ \mathbf{N}_{31} = \left(\lambda^2\Gamma_{pL} + \mu\Gamma_{sL}\right) / \beta_L\,,$$

$\mathbf{N}_{32} = 1 + \lambda^2 \Gamma_{sL} / \beta_L$, $\mathbf{N}_{33} = 1$, $\mathbf{N}_{41} = \lambda^2 \Gamma_{sL}$,
$\mathbf{N}_{43} = \lambda^2 \rho I'_x L^3 s^2 / EI_L$, $\mathbf{N}_{44} = \lambda^2 \rho L^2 s^2 / E + 1$.

Appendix

A.2

In Eq. (25), the elements of the matrices $\mathbf{F}_0(s_0)$ and $\mathbf{N}_0(s_0)$ vanish unless those that are displayed below.

$\mathbf{F}_{12} = \mathbf{F}_{34} = 1$, $\mathbf{F}_{21} = \Gamma_0 / \left(\lambda^2 \Gamma_0 + \beta_0\right)$,
$\mathbf{F}_{24} = -\beta_0 / \left(\lambda^2 \Gamma_0 + \beta_0\right)$, $\mathbf{F}_{42} = \beta_0 / \left(\lambda^2 \Gamma_0 \alpha_0 + 1\right)$,
$\mathbf{F}_{43} = \left(\Gamma_0 \alpha_0 + \beta_0\right) / \left(\lambda^2 \Gamma_0 \alpha_0 + 1\right)$.
$\mathbf{N}_{31} = \mu \Gamma_L / \beta_L$, $\mathbf{N}_{32} = \lambda^2 \Gamma_L / \beta_L + 1$, $\mathbf{N}_{33} = 1$, $\mathbf{N}_{41} = \lambda^2 \Gamma_L$,
$\mathbf{N}_{44} = \lambda^2 \Gamma_L \alpha_L + 1$.

In Eq. (26), the elements of the matrices $\mathbf{F}_1(X, s_0, s_1) = \mathbf{F}_{10} + \mathbf{F}_{11} s_1$ vanish unless those that are displayed below. For matrix $\mathbf{F}_{10}$ the corresponding elements are

$\mathbf{F}_{22} = -\left(2\lambda^2 \chi_L \Gamma_0 + \beta_0 \chi_L\right) / \left(\lambda^2 \Gamma_0 + \beta_0\right)$,
$\mathbf{F}_{23} = -\beta_0 \chi_L / \left(\lambda^2 \Gamma_0 + \beta_0\right)$, $\mathbf{F}_{42} = -\beta_0 \phi_x / \left(\lambda^2 \Gamma_0 \alpha_0 + 1\right)$,
$\mathbf{F}_{43} = -\beta_0 \phi_x / \left(\lambda^2 \Gamma_0 \alpha_0 + 1\right)$,
$\mathbf{F}_{44} = -4\mathrm{T}_0 \left(2\lambda^2 \Gamma_0 \alpha_0 + 1\right) / \left(\lambda^2 \Gamma_0 \alpha_0 + 1\right)$.

For matrix $\mathbf{F}_{11}$ the corresponding elements are

$\mathbf{F}_{21} = \Gamma_0 \beta_0 / \left(\Gamma_0 \lambda^2 + \beta_0\right)^2 / s_0$,
$\mathbf{F}_{24} = \lambda^2 \beta_0 \Gamma_0 / \left(\lambda^2 \Gamma_0 + \beta_0\right)^2 / s_0$,
$\mathbf{F}_{42} = -\lambda^2 \beta_0 \rho L^2 / \left(\lambda^2 \Gamma_0 \alpha_0 + 1\right)^2 / E$,
$\mathbf{F}_{43} = \left(1 - \lambda^2 \beta_0\right) \rho L^2 / \left(\lambda^2 \Gamma_0 \alpha_0 + 1\right)^2 / E$.

In Eq. (26), the elements of the matrices $\mathbf{N}_1(s_0, s_1) = \mathbf{N}_{10} + \mathbf{N}_{11} s_1$ vanish unless those that are displayed below. For matrix $\mathbf{N}_{10}$ the corresponding elements are

$\mathbf{N}_{31} = 2\lambda^2 L^5 \rho \delta \pi s_0 / \beta_L EI_L$, $\mathbf{N}_{43} = 4\lambda^2 L^2 \rho T_L s_0 / E$.

For matrix $\mathbf{N}_{11}$ the corresponding elements are

$\mathbf{N}_{31} = \mu \rho A_L L^4 / \beta_L EI_L$, $\mathbf{N}_{32} = \lambda^2 \rho A_L L^4 / \beta_L EI_L$,
$\mathbf{N}_{41} = \lambda^2 \rho A_L L^4 / EI_L$, $\mathbf{N}_{44} = \lambda^2 \rho L^2 / E$.

Hai-Li Tang received his M.S. degree from the National University of Defense Technology (NUDT), China, in 2013. Mr. Li is currently an engineer in the College of Aerospace Science and Engineering, NUDT. His research interests include vibration analyses of carbon nanotubes and Graphene sheets.

Daokui Li received his Ph.D. in solid mechanics from the National University of Defense Technology (NUDT), China, in 2002. From 2011 to 2012, he worked as a visiting scholar at the School of Engineering, University of Glasgow in the U.K. Dr. Li is currently a professor at the College of Aerospace Science and Engineering, NUDT. His research interests include composite structural mechanics and computational solid mechanics.